Second-harmonic spectroscopy of interband excitations at the interfaces of strained Si(100)-$Si_{0.85}Ge_{0.15}$-SiO_2 heterostructures

G. Erley
Institut für Grenzflächenforschung und Vakuumphysik, Forschungszentrum Jülich, D-52425 Jülich, Germany

R. Butz
Institut für Schicht- und Ionentechnik, Forschungszentrum Jülich, D-52425 Jülich, Germany

W. Daum
Institut für Grenzflächenforschung und Vakuumphysik, Forschungszentrum Jülich, D-52425 Jülich, Germany
(Received 17 July 1998)

We have applied optical second-harmonic generation to the spectroscopy of strained Si(100)-$Si_{0.85}Ge_{0.15}$-SiO_2 heterostructures, covering the full range of the fundamental critical-point interband transitions. By analyzing spectra from samples with different thicknesses of the alloy layer ranging from 4 to 28 nm, we were able to resolve different interband excitations localized at the two buried interfaces of this system. The contribution of the substrate-alloy interface to the spectra consists of bulklike, E_1- and E_2-type critical-point transitions, consistent with a pseudomorphic structure of this interface. The dominating excitations at the alloy-oxide interface, comprised of a broad resonance centered around 3.6 eV, have no equivalent in the bulk, and were also observed at Si(100)-SiO_2 interfaces. These transitions are assigned to alloy atoms without T_d symmetry at the boundary between the $Si_{0.85}Ge_{0.15}$ layer and the SiO_x transition region. [S0163-1829(99)13903-1]

I. INTRODUCTION

$Si_{1-x}Ge_x$ alloys represent an important class of semiconductor materials for microelectronic and optoelectronic applications, because their epitaxy is compatible with existing silicon wafer technology.[1] One promising application is the use of thin $Si_{1-x}Ge_x$ layers as the base material in heterobipolar transistors, which allow the realization of high-frequency devices without resorting to III-V technology.[2] As a consequence of their pseudomorphic growth on Si(100) substrates, such thin alloy layers exhibit tetragonal strain and a vertical lattice parameter larger than that of the unstrained Si substrate.[1] Since Ge content and strain affect the band structure and the energetic positions of the critical-point interband transitions, the bulk optical properties of both strained and relaxed alloy films have been extensively investigated.[3,4] However, the effect of the interfaces of Si-$Si_{1-x}Ge_x$ heterostructures on the interband transitions has not been explored so far, although interface properties become increasingly important as the thickness of the alloy layers is decreased.

In this paper we present a comprehensive second-harmonic generation (SHG) study of interband transitions at the interfaces of strained Si(100)-$Si_{0.85}Ge_{0.15}$-SiO_2 heterostructures. We used SHG to excite the transitions because this process is dipole forbidden in centrosymmetric materials such as Si and homogeneously strained $Si_{1-x}Ge_x$ alloys. As a consequence, SHG is very sensitive to the interfaces of Si-$Si_{1-x}Ge_x$ structures. Our spectra cover the full range (2–5 eV) of the fundamental critical-point interband transitions, enabling a detailed comparison with bulk optical spectra. With respect to previous spectroscopic SHG studies of semiconductor interfaces,[5–7] our present study features an additional interesting aspect of nonlinear interface optics: the Si(100)-$Si_{0.85}Ge_{0.15}$-SiO_2 heterostructures contain two buried interfaces which both generate the second harmonic resonantly. We demonstrate that the contributions of the two interfaces to the spectra can be resolved when spectra from samples with different thicknesses are analyzed. We observe very strong E_1-type interband excitations at the Si(100)-$Si_{0.85}Ge_{0.15}$ interface, leading to a dramatic increase of SHG intensity compared to the signals from Si(100)-SiO_2 interfaces. For the alloy-oxide interface, we report on a very different type of interband excitation which is also present at Si(100)-SiO_2 interfaces,[8] and which to our knowledge has not been observed in previous works using linear optical spectroscopies.

The organization of this paper is as follows: in Sec. II we report on the preparation of the Si(100)-$Si_{0.85}Ge_{0.15}$ heterostructures, and describe our experimental setup. In Sec. III we introduce the theoretical framework for SHG at interfaces of multilayer systems, and discuss a critical-point model for the frequency dependence of the second-harmonic susceptibility that we used for the analysis of the measured spectra. Our results for SHG from the heterostructures are presented, analyzed, and discussed in Sec. IV.

II. EXPERIMENT

A. Preparation of the heterostructures

Our heterostructures were grown under ultrahigh-vacuum conditions by molecular-beam epitaxy on *p*-doped, 1000-Ω cm Si(100) substrates, which were covered with a 200-nm Si buffer layer at 700 °C prior to the epitaxy of the $Si_{1-x}Ge_x$ layer at 600 °C. The Ge content x of all layers was

 ©1999 The American Physical Society

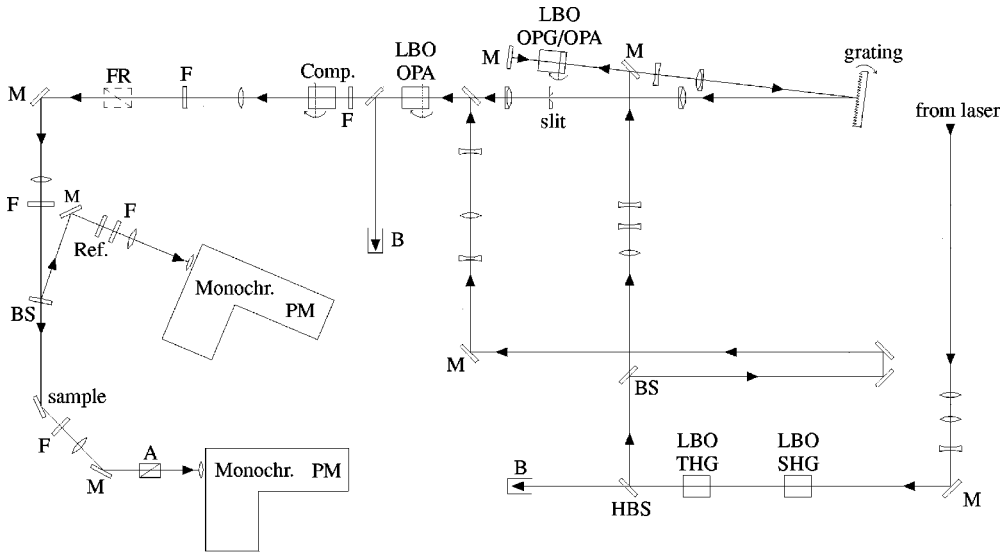

FIG. 1. Setup of the SHG laser spectrometer. *M*: mirror. SHG and THG: second- and third-harmonic converters. HBS: harmonic beam splitter. *B*: beam dump. BS: beam splitter. OPG/OPA: optical parametric generator/amplifier. Comp: compensator for vertical beam displacement. *F*: color filter, FR: Fresnel rhombs. Ref.: reference sample. *A*: analyzer. Monochr.: 1/8-m monochromator. PM: photomultiplier.

15%, as determined by Rutherford backscattering measurements. The surfaces of the structures were well ordered, exhibited $2\times n$ dimer reconstructions as revealed by scanning tunneling microscopy and low-energy electron diffraction, and did not expose more than three atomic layers.[9] Samples with different alloy thicknesses were grown in subsequent deposition runs under virtually identical conditions, locked out of the deposition chamber, and covered with a thin layer of native SiO_2 by exposure to air. Our heterostructures with alloy thicknesses between 4 and 28 nm were fully strained, as these thicknesses were well below the critical thickness for strain relaxation which is about 100 nm for a Ge concentration of 15%.[10] Unintentional *p*-type doping of the buffer and alloy layers was below 1×10^{16} cm^{-3}.

B. SHG laser spectrometer

Tunable, high-power light pulses for efficient excitation of second-harmonic photons with energies between 2 and 5 eV were produced by a picosecond optical-parametric converter system[11] (Fig. 1) similar to that described in Ref. 12. Pulses of 355-nm wavelength and 18-ps duration, obtained from a flashlamp-pumped, actively and passively mode-locked 10 Hz-Nd:YAG (yttrium aluminum garney) laser by third-harmonic generation, were used to pump the parametric converter consisting of two angle-tuned, type-I phase-matched Lithium triborate (LBO) crystals. The first LBO crystal was pumped with about 3-mJ pulse energy in a two-pass configuration. The signal wave generated in the first crystal was monochromatized to less than 3 meV bandwidth with a 2400 lines/mm holographic grating in a near-Littrow geometry, and parametrically amplified in a second LBO crystal which was pumped with about 6-mJ pulse energy. A rotatable glass block made of Infrasil quartz glass was used to compensate for the vertical beam displacements caused by the frequency tuning of the parametric converter. The tuning range of the parametric pulses with about 14-ps pulse duration was from 0.41 to 2.4 μm.

The *p*-polarized beam from the parametric converter was slightly focused onto the sample at an angle of incidence $\theta = 65°$. For experiments with *s*-polarized excitation, a pair of Fresnel rhombs was inserted into the beam. Undesired idler or signal radiation, second-harmonic light generated in optical components before the sample, and residual light at 0.355 nm were suppressed with appropriate glass filters. The polarization state of the detected second-harmonic photons was selected with a Rochon analyzer. After spectral filtering with appropriate glass filters and a 1/8 m monochromator, the second-harmonic photons were detected with a photomultiplier tube and a gated digitizing storage oscilloscope. Four different sets of glass filters were necessary to achieve sufficient suppression of the fundamental photons in the spectral range of these investigations (2.4–5.0 eV). The dark count rate was about two counts in 1000 laser pulses. A personal computer was used for data acquisition, for the wavelength control of the monochromators, and for the frequency tuning of the parametric converter by rotation of the parametric crystals and the grating with stepping motors.

SHG spectra were measured for energies of the second-harmonic photons between 2.4 and 5.0 eV. We have also checked the energy range from 1.6 to 2.4 eV, but none of the samples discussed in this paper yielded a discernible SHG signal in this range. Our spectra were limited to a maximum second-harmonic photon energy of 5.0 eV because appropriate filters for efficient suppression of the fundamental photons for higher second-harmonic energies were not available. Pulse energies at the sample were typically 120 μJ for idler wavelengths (spectral range 1.2–1.75 eV) and 200 μJ for signal wavelengths (spectral range 1.75–2.5 eV). The energy fluence at the sample was less than 10^{-2} J/cm^2. We have checked the fluence dependence of the SHG intensity in a spectrum of a Si(100)-SiO_2 interface in the range of the E_1 transitions (3.2–3.4 eV), and did not observe significant changes for different fluences of our 14-ps pulses. Strong effects at fluences of less than 10^{-4} J/cm^2 due to carrier-induced screening of dc electric-field-induced SHG at the

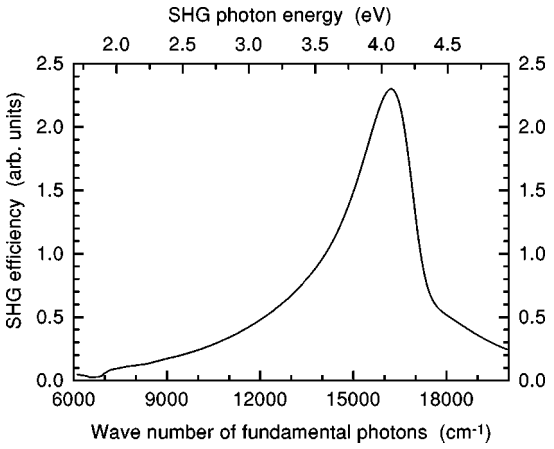

FIG. 2. SHG efficiency of the reference sample: urea crystallites with glycerol as an index-matching fluid.

$Si(100)$-SiO_2 interface have been reported previously in experiments with 110-fs laser pulses, however.[13]

C. SHG reference sample

To eliminate effects in the SHG spectra which are caused by laser power drift and by the wavelength dependence of both the pulse energies and of the spatial beam parameters, the sample spectra were normalized to the bulk SHG signal from a reference sample. About 7% of the beam power incident on the sample was deflected onto a reference sample consisting of a suspension of $20-40$-μm large urea crystallites in glycerol. Glycerol was used as an index-matching fluid to minimize scattering losses. The detection system for the reference signal was identical to the one for the sample signal. We used urea crystallites because of their large nonlinear coefficient and because of their capability of phase-matched SHG (Ref. 14) without introducing Maker oscillations as the frequency is tuned.

Because of noncritical type-II phase matching, the SHG efficiency of the urea crystallites has the spectral dependence shown in Fig. 2, with a strong maximum around 16 100 cm^{-1}, which has to be taken into account when normalizing sample spectra. The part of the spectrum between 15 200 and 20 000 cm^{-1} in Fig. 2 was determined experimentally[15] and fitted with a spline function. For frequencies below 15 200 cm^{-1}, where no experimental data were avalaible, we used the monotonic frequency dependence calculated from the theory of SHG in small phase-matchable crystallites.[11]

III. THEORETICAL FRAMEWORK AND DATA ANALYSIS

A. SHG in multilayer systems

In Fig. 3 we illustrate the general situation of SHG in a multilayer system. A laser beam with frequency ω is incident on the system. Contributions to the second-harmonic wave with frequency 2ω are generated at each interface and in the bulk of each layer. Reflection and transmission of both the pump wave and the second-harmonic wave occur at each interface. The outgoing second-harmonic wave whose power is detected in the experiment is a coherent superposition of

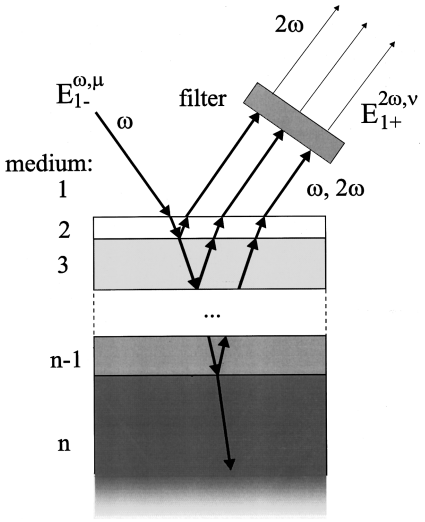

FIG. 3. SHG in a multilayer system. $E_{1^-}^{\omega,\mu}$ and $E_{1^+}^{2\omega,\nu}$ denote the electric-field amplitudes of the incoming μ-polarized fundamental wave and the outgoing ν-polarized second-harmonic wave, respectively, in medium 1.

the contributions from all interfaces and layers. A quantitative analysis of SHG spectra from heterostructures therefore necessitates a model of the SHG response that takes into account all linear optical effects of the propagating fundamental and second-harmonic waves such as multiple reflections at the interfaces and absorption in the layers.

For this purpose, we have extended the matrix formalism developed by Sipe for the low-index (100), (110), and (111) surfaces of cubic crystals[16,17] to multilayer sytems.[11] Our model considers SHG at all relevant interfaces of the system, quadrupole-type SHG in the bulk of the centrosymmetric layers, and dc-field-induced SHG if the electrostatic field of a space-charge region near an interface is sufficiently strong. Following Ref. 18, we use in our description of SHG at interfaces an effective second-harmonic interface susceptibility defined by

$$\chi_{s,\alpha\beta\gamma}^{(2)}(\omega,\omega) := \int_{\text{interface}} dz\, dz'\, dz''\, \chi_{\alpha\beta\gamma}^{(2)} \times (z,z',z'';\omega,\omega) s_\alpha^{2\omega}(z) s_\beta^{\omega}(z') s_\gamma^{\omega}(z''), \tag{1}$$

where z is the coordinate normal to the interface, and $\chi_{\alpha\beta\gamma}^{(2)}(z,z',z'';\omega,\omega)$ is the nonlocal and frequency-dependent second-harmonic susceptibility integrated over the coordinates x and y parallel to the interface. The functions $s_\alpha^{2\omega}(z), s_\alpha^{\omega}(z)$ are defined as (Systeme International units)

$$s_\alpha^{\Omega}(z) := \begin{cases} 1 & \text{for } \alpha \in \{x,y\} \\ \epsilon_0 E_z^{\Omega}(z)/D_z^{\Omega}(z_0) & \text{for } \alpha = z, \end{cases} \tag{2}$$

with $\Omega = 2\omega$ or ω. The component $E_z^{\Omega}(z)$ of the electric-field strength perpendicular to the interface varies rapidly across the interface, while the perpendicular component $D_z^{\Omega}(z_0)$ of the dielectric displacement is continuous at, and practically constant within, the transversal extension of the interface. $z = z_0$ defines an arbitrary plane within the interface. In writing Eqs. (1) and (2) we assume that the thickness of the interface region is small compared to the second-harmonic wavelength and also small compared to the absorp-

tion lengths for both the fundamental and second-harmonic photons. The continuous field components $D_z^{\Omega}(z_0), E_x^{\Omega}(z_0)$, and $E_y^{\Omega}(z_0)$ are then determined by the dielectric functions $\epsilon(\Omega)$ of the bulk media adjacent to the interface. With this definition of $\chi^{(2)}_{s,\alpha\beta\gamma}(\omega,\omega)$, the second-harmonic interface polarization (dimension: dipole moment per area) at z_0 can be written as

$$P^{2\omega}_{s,\alpha}(z_0)=\epsilon_0\sum_{\beta\gamma}\chi^{(2)}_{s,\alpha\beta\gamma}(\omega,\omega)F^{\omega}_{\beta}(z_0)F^{\omega}_{\gamma}(z_0), \qquad (3)$$

with

$$F^{\omega}_{\alpha}(z):=\begin{cases} E^{\omega}_{\alpha}(z) & \text{for } \alpha\in\{x,y\} \\ D^{\omega}_{\alpha}(z)/\epsilon_0 & \text{for } \alpha=z. \end{cases} \qquad (4)$$

For tensor elements of $\chi^{(2)}$ with one or more indices equal to z, the interface susceptibility $\chi^{(2)}_{s,\alpha\beta\gamma}$ defined in Eqs. (1) and (2), is a somewhat peculiar hybrid because it depends not only on the nonlinear optical response $\chi^{(2)}_{\alpha\beta\gamma}(z,z',z'';\omega,\omega)$ of the interface but also on the variation of the electric-field strength E_z across the interface. Although it would be desirable to separate between linear and nonlinear optical effects of an interface in a SHG spectrum, only the quantity $\chi^{(2)}_{s,\alpha\beta\gamma}$ can be directly determined in a SHG experiment because the variation of E_z across the interface is generally unknown.

For (100)- and (111)-oriented interfaces of multilayer systems with cubic bulk symmetry, the tensor elements $\chi^{(2)}_{s,zzz}, \chi^{(2)}_{s,zxx}, \chi^{(2)}_{s,xxz}$, and $\chi^{(2)}_{s,xxx}$ [the latter is nonzero only for the (111) orientation] of the effective interface suceptibility contribute to the SHG. In addition to SHG at interfaces, a second-harmonic wave is also generated in the bulk of centrosymmetric materials through a nonlocal, electric-quadrupole-type bulk polarization

$$P^{2\omega}_{b,\alpha}(\mathbf{r})=\epsilon_0[\gamma\nabla_{\alpha}[E^{\omega}(\mathbf{r})^2]+\zeta E^{\omega}_{\alpha}(\mathbf{r})\nabla_{\alpha}E^{\omega}_{\alpha}(\mathbf{r})], \qquad (5)$$

with γ and ζ being the isotropic and anisotropic nonlocal bulk SHG coefficients, respectively, for cubic crystals.[16] We also consider dc-field-induced bulk SHG according to

$$P^{2\omega}_{b,\alpha}(\mathbf{r})=\epsilon_0\sum_{\beta\gamma}\chi^{(3)}_{\alpha\beta\gamma z}(\omega,\omega,0)E^{\omega}_{\beta}(\mathbf{r})E^{\omega}_{\gamma}(\mathbf{r})E^{dc}_{z}(z), \qquad (6)$$

where $\chi^{(3)}_{\alpha\beta\gamma z}(\omega,\omega,0)$ is a third-order nonlinear susceptibility and $E^{dc}_z(z)$ the electrostatic field strength in the space-charge region.[19–21]

The ν-polarized amplitude $E^{2\omega,\nu}_{1+}$ of the outgoing second-harmonic wave generated in the multilayer system and reflected back to medium 1 (vacuum or air) is related to the μ-polarized amplitude $E^{\omega,\mu}_{1-}$ of the ingoing pump wave incident from medium 1 onto the system of layers 2 to n (layer n being the substrate, see Fig. 3) through the interface and bulk second-harmonic susceptibility tensor elements $\chi_{i,j}(\omega,\omega)$ of all layers $i=2$ to n, multiplied with appropriate coefficients $a_{\mu\nu}, b_{\mu\nu}$ and $c_{\mu\nu}$:

$$E^{2\omega,\nu}_{1+}=\sum_{i=2}^{n}\sum_{j}[a_{\mu\nu}(\chi_{i,j})+b_{\mu\nu}(\chi_{i,j})\sin m\phi + c_{\mu\nu}(\chi_{i,j})\cos m\phi]\chi_{i,j}(E^{\omega,\mu}_{1-})^2. \qquad (7)$$

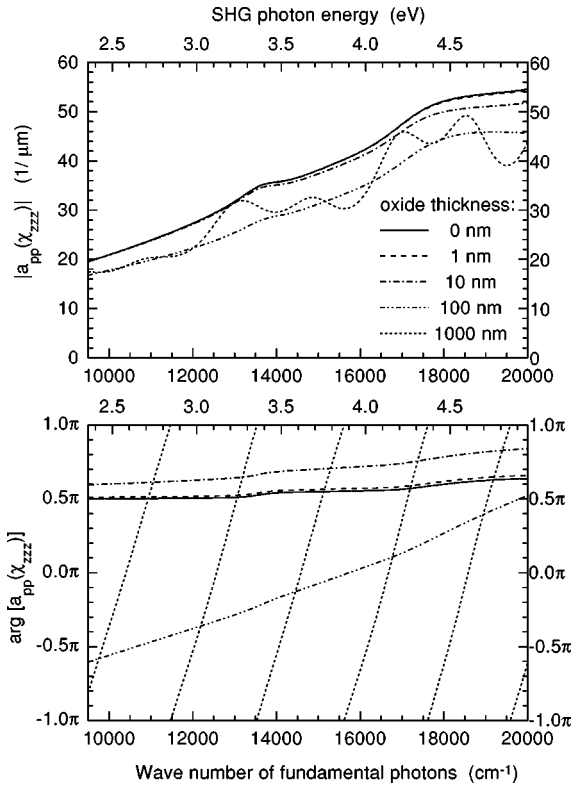

FIG. 4. Magnitude and phase of the SHG coefficient $a_{pp}(\chi^{(2)}_{s,zzz})$ for the Si-SiO_2 interface, calculated for different oxide thicknesses.

The j summation includes all relevant elements of the second-harmonic susceptibility tensors in Eqs. (3), (5), and (6). Both, the variation of these coefficients with frequency, which can be calculated if the dielectric functions $\epsilon_i(\omega)$ and $\epsilon_i(2\omega)$ of all layers $i=2$ to n are known, and their variation with the angle of incidence θ depend on the tensor element $\chi_{i,j}$. Furthermore, the terms with the coefficients $b_{\mu\nu}$ and $c_{\mu\nu}$ introduce a dependence of the second-harmonic field strength on the azimuthal orientation (angle ϕ) of the sample, with a threefold symmetry ($m=3$) for systems with (111) orientation, and a fourfold symmetry ($m=4$) for systems with (100) orientation.

The matrix formalism for the calculation of the SHG coefficients in Eq. (7) automatically takes care of multiple reflections in the layers.[17] The importance of multiple reflections for sufficiently thick layers is demonstrated in Fig. 4, where the frequency dependence of both the magnitude and phase of the coefficient $a_{pp}(\chi^{(2)}_{s,zzz})$ is shown, as calculated for Si-SiO_2 systems with different oxide thicknesses. For the dielectric function of SiO_2 we have used the data of Ref. 22. The effect of very thin oxides $\leqslant 1$ nm on the propagation of the beams is completely negligible, while the effect of the oxide is clearly discernible for oxide thicknesses >10 nm. For very thick layers $\gg 100$ nm, strong oscillations of the magnitude and rapid phase changes modulate the frequency dependence of the nonlinear susceptibility in a SHG spectrum.

Absorption of the pump and the second-harmonic wave, which is fully taken into account by the SHG coefficients, can also affect the frequency dependence of a SHG spectrum in a dramatic way. As an example relevant to the subsequent discussion of SHG spectra from Si(100)-$Si_{0.85}Ge_{0.15}$-SiO_2 heterostructures, in Fig. 5 we show the cal-

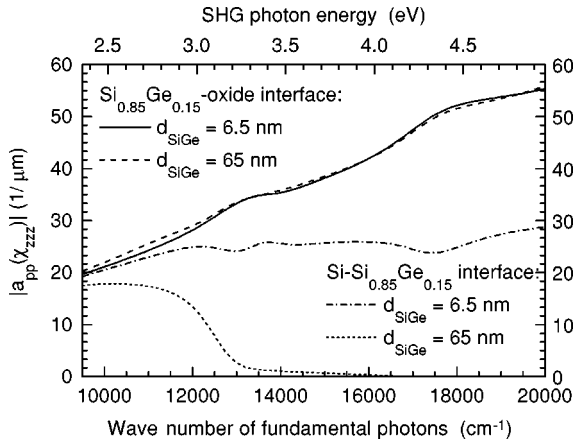

FIG. 5. Magnitude of the SHG coefficient $a_{pp}(\chi^{(2)}_{s,zzz})$ of the two buried interfaces of a Si-$Si_{0.85}Ge_{0.15}$-SiO_2 system, calculated for alloy layer thicknesses of 6.5- and 65-nm, respectively, and for an oxide thickness of 1 nm. The small differences of $a_{pp}(\chi^{(2)}_{s,zzz})$ of the $Si_{0.85}Ge_{0.15}$-oxide interface with 6.5- and 65-nm alloys are due to different multiple reflections in the alloy layers.

culated frequency dependence of $|a_{pp}(\chi^{(2)}_{s,zzz})|$ for both the $Si_{0.85}Ge_{0.15}$-oxide interface, and the Si-$Si_{0.85}Ge_{0.15}$ interface, and for alloy layers of 6.5 and 65 nm. For the dielectric function of $Si_{0.85}Ge_{0.15}$ we used interpolated data from Ref. 3. As expected, the coefficient for the contribution from the upper interface is virtually independent of the alloy thickness, while the coefficient for the lower interface dramatically decreases with layer thickness for second-harmonic photon energies above 3 eV due to strong interband absorption in the alloy.

B. Critical point interband resonances in SHG

So far we have not considered the frequency dependence of the nonlinear susceptibility which is resonantly enhanced for excitation of interband transitions with a high joint density of states. In what follows we discuss our resonance model for the nonlinear susceptibility which we used in our analysis of the experimental data, and which allowed us to extract relevant material parameters such as the critical-point (CP) energies at interfaces. The second-harmonic susceptibility of crystalline semiconductors and insulators can be expressed in terms of direct optical interband transitions:[23]

$$\chi^{(2)}_{\alpha\beta\gamma}(\omega,\omega)=\sum_{v,c,c'}\int d\mathbf{k}\frac{\langle v,\mathbf{k}|d_\alpha|c,\mathbf{k}\rangle}{\hbar[2\omega-\omega_{cv}(\mathbf{k})]}\times A^{v,c,c'}_{\beta\gamma}(\mathbf{k};\omega,\omega)f[E_\nu(\mathbf{k}),T]+(\text{nonresonant contribution}) \quad (8)$$

with $\hbar\omega_{cv}=E_c(\mathbf{k})-E_v(\mathbf{k})$,

$$A^{v,c,c'}_{\beta\gamma}(\mathbf{k};\omega,\omega)=\frac{\langle c,\mathbf{k}|d_\beta|c',\mathbf{k}\rangle\langle c',\mathbf{k}|d_\gamma|v,\mathbf{k}\rangle}{\hbar[\omega-\omega_{c'v}(\mathbf{k})]}+\frac{\langle c,\mathbf{k}|d_\gamma|c',\mathbf{k}\rangle\langle c',\mathbf{k}|d_\beta|v,\mathbf{k}\rangle}{\hbar[\omega-\omega_{c'v}(\mathbf{k})]}, \quad (9)$$

and $f[E_\nu(\mathbf{k}),T]$ being the Fermi distribution. The quantum numbers v,c,c', and $\mathbf{k}$ denote the valence- and conduction-band indices, respectively, and the wave vector in the first Brillouin zone of the crystal. $\mathbf{d}=-e\mathbf{r}$ is the electric dipole moment operator. In separating the nonlinear susceptibility in Eq. (8) into resonant and nonresonant parts, we make use of the fact that for the frequency range of our exciting laser photons (1.2–2.5 eV) resonant excitation of direct interband transitions in the Si-$Si_{0.85}Ge_{0.15}$ system is not possible with the fundamental frequency ω. Only the two-photon frequencies 2ω fall in the spectral range of the interband transitions $|c,\mathbf{k}\rangle\rightarrow|v,\mathbf{k}\rangle$. As a consequence, the frequency dependence of $A^{v,c,c'}_{\beta\gamma}(\mathbf{k};\omega,\omega)$ is weak and can be neglected for our purposes. Note that for a dipole-allowed transition $|c,\mathbf{k}\rangle\rightarrow|v,\mathbf{k}\rangle$ in centrosymmetric crystals such as Si, the products of the two matrix elements in Eq. (9) [and corresponding products appearing in the nonresonant contribution in Eq. (8), see Ref. 23] are zero because either $|c,\mathbf{k}\rangle$ and $|c',\mathbf{k}\rangle$ or $|c',\mathbf{k}\rangle$ and $|v,\mathbf{k}\rangle$ have the same parity.

As far as CP transitions are concerned, only a limited range $\{\mathbf{k}_r\}$ of $\mathbf{k}$ vectors of the Brillouin zone contributes significantly to a particular CP labeled with the index r. $A^{v,c,c'}_{\beta\gamma}(\mathbf{k};\omega,\omega)$ may therefore be averaged over this part of the Brillouin zone. The resonant part of $\chi^{(2)}_{\alpha\beta\gamma}(\omega,\omega)$ can then be written as a superposition of CP's:

$$\chi^{(2)}_{\alpha\beta\gamma}(\omega,\omega)\approx\sum_{r(CP's)}B^r_{\beta\gamma}(\omega,\omega)\times\int_{\mathbf{k}_r}d\mathbf{k}\frac{\langle v_r,\mathbf{k}|d_\alpha|c_r,\mathbf{k}\rangle}{\hbar[2\omega-\omega_{c_rv_r}(\mathbf{k})]}f[E_\nu(\mathbf{k}),T]+(\text{nonresonant contribution}), \quad (10)$$

with

$$B^r_{\beta\gamma}(\omega,\omega)=\sum_{c'}\overline{A^{c'c_rv_r}_{\beta\gamma}(\mathbf{k};\omega,\omega)}^{\mathbf{k}_r}. \quad (11)$$

The range of integration in Eq. (10) and the $\mathbf{k}$ range of averaging in Eq. (11) refer to that part of the Brillouin zone which contributes significantly to the CP with index r. Neglecting again the $\mathbf{k}$ dependence of the matrix element in Eq. (10) for a particular CP, the integral in Eq. (10) represents the resonant part of the CP contribution to the linear dielectric function,

$$\epsilon(2\omega)=\sum_r\epsilon_r(2\omega), \quad (12)$$

with

$$\epsilon_r(\omega)=\int_{\mathbf{k}_r}d\mathbf{k}\frac{|\langle v_r,\mathbf{k}|d_\alpha|c_r,\mathbf{k}\rangle|^2}{\hbar[\omega-\omega_{c_rv_r}(\mathbf{k})]}\,f[E_{\nu_r}(\mathbf{k}),T]. \quad (13)$$

The CP structures in $\epsilon(\omega)$ spectra of semiconductors are commonly analyzed in terms of standard analytic line shapes[24]

$$\epsilon_r(\omega)=C_r-f_re^{i\psi_r}(\omega-E_r/\hbar+i\Gamma_r)^{n_r}, \quad (14)$$

with f_r being the amplitude, ψ_r the excitonic phase angle, E_r the energy, and Γ_r the broadening of the CP resonance. The index n_r can assume various values, depending on the type of CP. In particular, the case $n_r=-1$ is referred to as exci-

tonic line shape which represents the best fit to the E_1 CP of bulk Si.[24] Using Eqs. (10)–(14), one can derive an expression for $\chi^{(2)}_{\alpha\beta\gamma}(\omega,\omega)$ in terms of CP resonances:

$$\chi^{(2)}_{\alpha\beta\gamma}(\omega,\omega)\approx\sum_r \tilde{B}^r_{\beta\gamma}(\omega,\omega) f_r e^{i\psi_r}(2\omega-E_r/\hbar+i\Gamma_r)^{n_r} + (\text{nonresonant contribution}), \quad (15)$$

with

$$\tilde{B}^r_{\beta\gamma}(\omega,\omega)=-B^r_{\beta\gamma}(\omega,\omega)\overline{\langle c_r,\mathbf{k}|d_\alpha|v_r,\mathbf{k}\rangle}^{\mathbf{k}_r}. \quad (16)$$

According to Eq. (15), the second-harmonic susceptibility exhibits a frequency dependence which is very similar to the CP structure of the linear dielectric function $\epsilon(2\omega)$, provided the fundamental frequency is sufficiently away from all CP resonances so that the frequency dependence of $\tilde{B}^r_{\beta\gamma}(\omega,\omega)$ is sufficiently weak.

The above discussion of the frequency dependence $\chi^{(2)}_{\alpha\beta\gamma}$ directly applies to bulk SHG in crystals without inversion symmetry such as GaAs. In centrosymmetric crystals like Si or $Si_{0.85}Ge_{0.15}$, SHG is dipole allowed only at interfaces. Close to interfaces, the wave vector $\mathbf{k}$ is not a good quantum number and should be replaced by the wave vector $\mathbf{k}_\parallel$ parallel to the interface and by l_z, the label of atomic layers perpendicular to the interface. If the bonding at interfaces is not too different from the bulk, the perturbation of bulklike states at the interface is moderate, and the $(\mathbf{k}_\parallel,l_z)$ equivalent to Eq. (13) has a similar CP-type frequency dependence. More dramatic differences can be expected for the matrix elements of $A^{v,c,c'}_{\beta\gamma}(\mathbf{k}_\parallel,l_z,\omega,\omega)$ in Eq. (9) because the modified bonding at the interface is exactly the reason for finite values of the matrix elements, yielding a nonzero $\chi^{(2)}_{s,\alpha\beta\gamma}$. Since the perturbation of the bulk states decreases with increasing distance from the interface, the magnitude of $A^{v,c,c'}_{\beta\gamma}(\mathbf{k}_\parallel,l_z,\omega,\omega)$ also decreases for layers farther away from the interface. Therefore, the factor $A^{v,c,c'}_{\beta\gamma}(\mathbf{k}_\parallel,l_z,\omega,\omega)$ in Eq. (8) weighs the contributions of the layers closer to the interface more strongly.

Notwithstanding this complication for interface susceptibilities, we found that E_1- and E_2-type interface resonances in our SHG spectra could be reasonably well described by Eq. (15) with $n_r=-1$.[8] Inserting this frequency dependence for the second-harmonic susceptibility into Eq. (7), one obtains, for the SHG intensity,

$$I(2\omega)\propto\left|\sum_{k=1}^{n} A_k(\omega,\theta)\frac{f_k\exp(i\psi_k)}{2\omega-\omega_k+i\Gamma_k}\right|^2, \quad (17)$$

where all relevant resonances at the interfaces and in the bulk of the multilayer system are considered in the summation. In writing Eq. (17) we neglect the frequency dependence of the coefficient $\tilde{B}^r_{\beta\gamma}$ in Eq. (15). The functions $A_k(\omega,\theta)$ represent the linear-optical coefficients $a_{\mu\nu}$, $b_{\mu\nu}$, and $c_{\mu\nu}$ in Eq. (7) that take into account the propagation of the fundamental and the second-harmonic wave through the system. For the analysis of our measured SHG spectra we performed least-square fits of the parameters in Eq. (17) using a Levenberg-Marquardt algorithm.[25] Our software allows us to specify the geometrical and bulk dielectric properties of a multilayer system, to assign resonances to the susceptibility tensor elements of the various interfaces or, in the case of quadrupole or dc-field-induced bulk SHG, of the bulk of the layers, and to fit the $(4n-1)$ parameters for n resonances until convergence is obtained. To optimize the fits we allowed the layer thickness to deviate by ± 0.5 nm from the nominal thickness. These deviations are within the accuracy of the determination of the layer thickness of the prepared structures. The stability of the fits was checked by repeating the procedures with different starting values for the parameters.

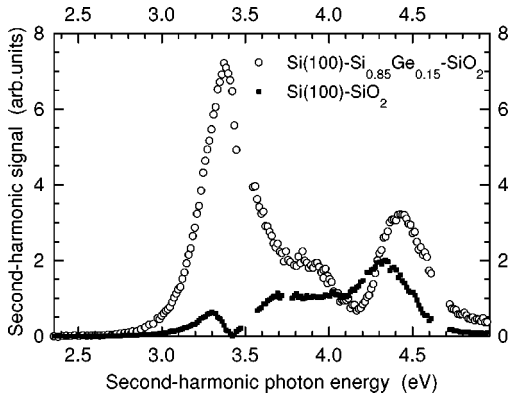

FIG. 6. SHG spectrum of a Si(100)-$Si_{0.85}Ge_{0.15}$ heterostructure with a 4-nm strained layer covered with a native oxide (open symbols), in comparison with the spectrum of a bare Si(100) sample also covered with a native oxide (full symbols).

We did not attempt to optimize the fits by introducing CP line shapes different from that in Eq. (17). We consider the fits as a means to determine the resonance parameters from the measured spectra, but we do not discuss physical implications of the CP line shape. The error margins of the fit parameters, in particular of the resonance energies, mainly originate from the unknown relative weight of the susceptibility tensor elements $\chi^{(2)}_{s,zzz}$, $\chi^{(2)}_{s,xxz}$, and $\chi^{(2)}_{s,zxx}$ in the SHG spectra (see the discussion in Sec. IV C). Thus an optimization of the line shape for the SHG resonances makes little sense at this level.

IV. RESULTS AND DISCUSSION

A. Si(100) -$Si_{0.85}Ge_{0.15}$-SiO_2 vs Si(100)-SiO_2

In Fig. 6 we show the SHG spectrum of a Si(100)-$Si_{0.85}Ge_{0.15}$-SiO_2 heterostructure with a 4-nm alloy layer, in comparison with the spectrum of a bare Si(100) sample (p doped, $2-10$ kΩ cm) covered with a native oxide. Both spectra were obtained using p-polarized light and detecting the p-polarized second harmonic. A remarkable result in Fig. 6 is the surprisingly strong intensity of the band around 3.37 eV from the heterostructure, exceeding that of the Si-SiO_2 interface by one order of magnitude, and pointing to a large optical nonlinearity of the alloy layer or of its interfaces.

The electrostatic field of the space-charge region, which has been shown to be an important source of SHG at semiconductor interfaces for sufficiently strong fields,[19–21] cannot be the primary cause for the SHG from our heterostructure for the following reason: with a valence-band discontinuity of 0.11 eV for the Si(100)-$Si_{0.85}Ge_{0.15}$ interface[26] and the

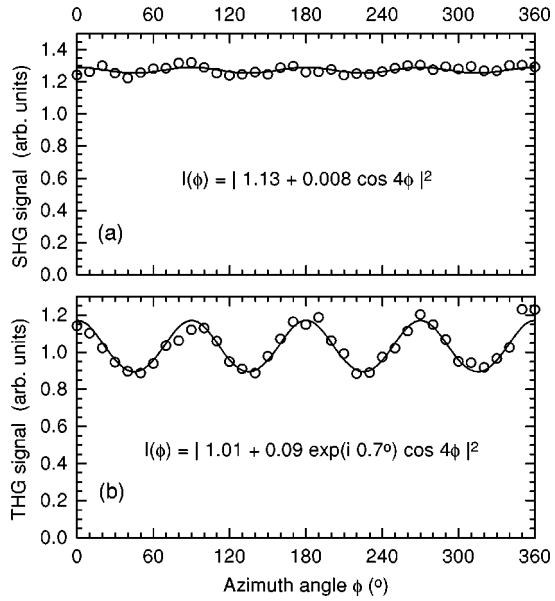

FIG. 7. (a) Azimuthal dependence of SHG at 3.22 eV from a 6.5-nm Si(100)-$Si_{0.85}Ge_{0.15}$ heterostructure. (b) Azimuthal dependence of THG at 3.4 eV from the same sample. Solid lines in (a) and (b): fits to the data with an isotropic contribution and an anisotropic contribution of C_{4v} symmetry. The results of the fits are also indicated.

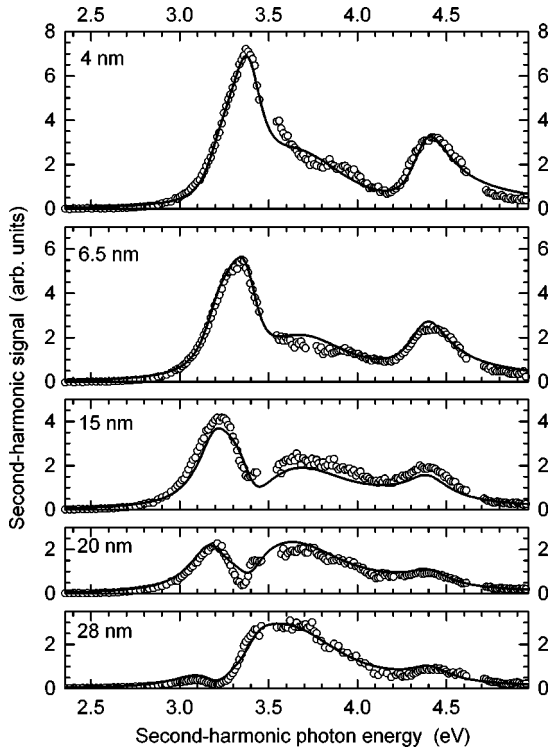

FIG. 8. SHG spectra of strained Si(100)-$Si_{0.85}Ge_{0.15}$-SiO_2 structures with the thickness of the alloy layer increasing from 4 to 28 nm (symbols). Solid lines: fit of CP-type interband resonances to the data, using the SHG coefficient for $\chi^{(2)}_{s,zzz}$.

dopant concentration quoted above, we estimate an electric-field strength of some kV/cm, too weak to produce the strong SHG signal of the 4-nm sample in Fig. 6. Band bending caused by interface states at the $Si_{0.85}Ge_{0.15}$–native-oxide interface affects the SHG efficiency in a similar manner as the Si–native-oxide interface does, and it cannot be responsible for the strong SHG from the heterostructure either. Also, quadrupole-type bulk SHG is comparatively small. Azimuthal SHG measurements at 3.22 eV on a 6.5-nm sample revealed that the magnitude of the anisotropic quadrupole bulk contribution (ζ) to the SHG signal from structures with a thin layer amounts to less than 1% of the total isotropic contribution [Fig. 7(a)]. Since the bulk linear dielectric functions of Si and $Si_{0.85}Ge_{0.15}$ are rather similar,[3,4] we also expect comparable isotropic bulk quadrupole susceptibilities γ for the two materials which cannot explain the dramatic intensity differences in Fig. 6. An upper limit for the contribution of γ was obtained from *s*-in/*p*-out measurements of hydrogen-terminated Si(111) surfaces[27] which probe γ together with ζ and the surface tensor element $\chi^{(2)}_{s,zxx}$. These measurements yielded intensities around 3.4 eV that were weaker than those from the heterostructure in Fig. 6 by a factor of about 250. Considering the stronger radiation efficiency of the *p*-in/*p*-out configuration, this signal causes an intensity of 0.17 on the scale of Fig. 6. Thus we can rule out both dc-field-induced and quadrupole-type bulk SHG to be responsible for the strong SHG signal in Fig. 6.

It should be noted that the lack of a pronounced crystalline anisotropy of the SHG signal from the heterostructure is not an indication of poor structural quality of the alloy layer but a consequence of the overall C_{4v} symmetry of the (100)-oriented material: only the comparatively weak quadrupole bulk polarization causes anisotropy in SHG, while the response from its interfaces is isotropic for systems with C_{4v} symmetry.[16] The crystalline anisotropy of the layer was, however, revealed in third-harmonic generation (THG) experiments. THG is dipole allowed in the bulk of the heterostructure, and exhibited the expected fourfold anisotropy in azimuthal measurements,[28] as shown in Fig. 7(b) for a third-harmonic photon energy of 3.4 eV.

B. Thickness dependence of the spectra

Further insight into the origin of the SHG from the heterostructures can be gained by comparing in Fig. 8 spectra from strained heterostructures with different thicknesses of the alloy layer ranging from 4 to 28 nm. The spectra exhibit pronounced variations of the intensity and spectral dependencies as a function of thickness. In particular, the intensities of the E_1- and E_2-type resonances *decrease* with increasing layer thickness. This result lends further support to our conclusion that SHG in the bulk of the strained alloy layers is not responsible for the strong SHG signal from the heterostructures. Furthermore, if SHG in the bulk of the layers were the dominant effect, the E_1 resonance energy should be close to the bulk value of 3.19 eV for strained $Si_{0.85}Ge_{0.15}$,[29] in contrast to the measured spectral position of the E_1-type feature at about 3.37 and 3.32 eV for the 4- and 6.5-nm heterostructures, respectively (Fig. 8).

The spectral position of this feature shifts from 3.37 eV for 4 nm to 3.20 eV for 20 nm, whereas the energy of the E_2-type feature remains constant at about 4.4 eV. We will show below that the spectra and their dependence on the alloy thickness are readily explained by interference of reso-

nant SHG at the outer alloy-oxide interface with SHG at the inner substrate-alloy interface. The escape depth of the SHG photons (see also Fig. 5), decreases from 14 nm at 3.2 eV to 4.4 nm at 4.3 eV in $Si_{0.85}Ge_{0.15}$.[3] The spectra for thin layers $\leqslant$6.5 nm are, therefore, dominated by strong SHG from the substrate-alloy interface, while the SHG from the 28 nm sample originates from the alloy-oxide interface for energies above the E_1 transitions.

C. Analysis and interpretation of the spectra

Ruling out significant contributions of quadrupole-type and dc-field-induced SHG in the bulk of the samples, we consider the interfaces of the heterostructures as the dominant radiation sources for the SHG spectra in Fig. 8. Consequently, the resonant structures in Fig. 8 must be related to resonant excitations of interband transitions at these interfaces.

As discussed in more detail elsewhere,[8] the frequency dependence of SHG at Si(100)-SiO_2 interfaces between 2 and 5 eV is caused by three different types of interband resonances: E_1- and E_2-type resonances at about 3.3 and 4.4 eV, respectively, and a third band around 3.7 eV specific to the Si(100)-SiO_2 interface. In analogy to the Si-SiO_2 interface, we have to consider three corresponding types of resonances for the $Si_{0.85}Ge_{0.15}$-SiO_2 interface as well. For the substrate-alloy interface only E_1- and E_2-type excitations are relevant because it is pseudomorphic. In contrast to the alloy-oxide interface, however, both adjacent regions of this interface are expected to contribute to the SHG. Since the bulk E_2 CP energy is virtually independent of the Ge content,[3,4] we can model the frequency dependence of the nonlinear interface susceptibility $\chi_s^{(2)}$ in this spectral region with a single resonance. The E_1 CP energy depends on the Ge content: 3.40 eV for Si,[24] and 3.19 eV for strained $Si_{0.85}Ge_{0.15}$ (Ref. 29) at 300 K. Therefore we describe the nonlinear response of this interface around E_1 with two resonances of $\chi_s^{(2)}$, representing interband transitions at either side of the interface.

Using the analytic form in Eq. (17), we have fitted the $(6\times4)-1$ independent parameters of the $n=6$ resonances described above simultaneously to all five spectra of Fig. 8, assuming that the set of the four parameters f_k, ω_k, γ_k, and ψ_k of each interface resonance does not change with the thickness of the alloy layer. The result is shown as solid lines in Figs. 8 and 9 using the coefficients $A_k(\omega,\theta)$ for the tensor element $\chi^{(2)}_{s,zzz}$ and $\chi^{(2)}_{s,xxz}$, respectively. Fits of similar quality as in Fig. 9 have also been obtained with the coefficient of the tensor element $\chi^{(2)}_{s,zxx}$. Considering the assumptions made about the line shapes and the fact that we used the same set of resonance parameters for five different samples (with only $23:5=4.6$ free fit parameters for one spectrum from 2 to 5 eV), the overall agreement between experiment and fit in Figs. 8 and 9 is quite satisfactory. A more realistic line shape for the band around 3.6 eV should improve the fits particularly for the 20- and 28-nm samples. We point out that the thickness of the alloy layer is the only parameter which is different for the five calculated spectra in Figs. 8 and 9. Thus it is clear that the pronounced dependence of the spectra on alloy thickness is predominantly caused by the optical propagation, i.e., interference and absorption, of the second-harmonic radiation generated at the two interfaces.

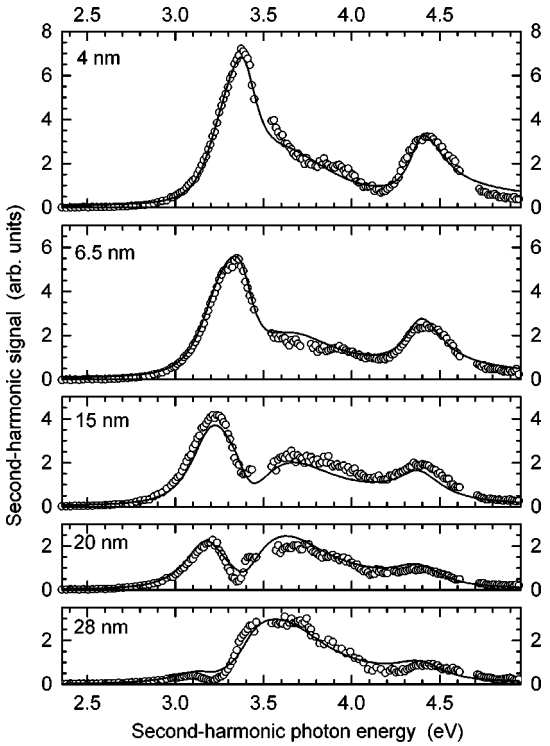

FIG. 9. Same as in Fig. 8, but with a fit for the tensor element $\chi^{(2)}_{s,xxz}$.

It should be noted that all three interface tensor elements $\chi^{(2)}_{s,zzz}$, $\chi^{(2)}_{s,xxz}$, and $\chi^{(2)}_{s,zxx}$ are probed with the p-in/p-out configuration. A separate measurement of $\chi^{(2)}_{s,xyz}$ using mixed-in/p-out polarizations was not attempted in this work. While s-in/p-out experiments on a 6.5-nm sample have indicated that $\chi^{(2)}_{s,zxx}$ alone cannot account for the measured SHG intensities in Fig. 8, its contribution to the spectra in Fig. 8 is not negligible.

The fit function in Eq. (17) includes only those interband transitions which are nearly resonant with the second-harmonic photon frequency 2ω. To explore possible effects of nonresonant contributions due to interband transitions at energies above the E_2 CP and due to nonresonant excitation with the fundamental photon frequency ω, we have simulated the nonresonant contribution in Eq. (15) by one additional resonance from each of the two interfaces with a very weak spectral dependence (resonance energy 5.0 eV, full width at half maximum 5.0 eV). Inclusion of these nonresonant contributions did not improve the fits significantly, and their maximum SHG intensity at 5.0 eV was less than 0.4 on the scale of the spectra in Fig. 8. Their very weak effect on the resonance energies is thus within the error margins of the fitted resonance energies quoted below.

More detailed information about the interband excitations at the two interfaces can be gathered from Figs. 10–12. The various contributions of the two interfaces to the spectra are displayed for the 4- and 28-nm heterostructures as the magnitude $|E^{2\omega}_{1+}|$ [see Eq. (7)] of the second-harmonic field strengths outside of the sample. These contributions were separately calculated from the fitted parameter values of each individual resonance assuming the SHG coefficients for $\chi^{(2)}_{s,zzz}$, $\chi^{(2)}_{s,xxz}$, and $\chi^{(2)}_{s,zxx}$, respectively. Except for the energy of the E_1-type resonance of the alloy-oxide interface, all three fits yield comparable results. The differences result

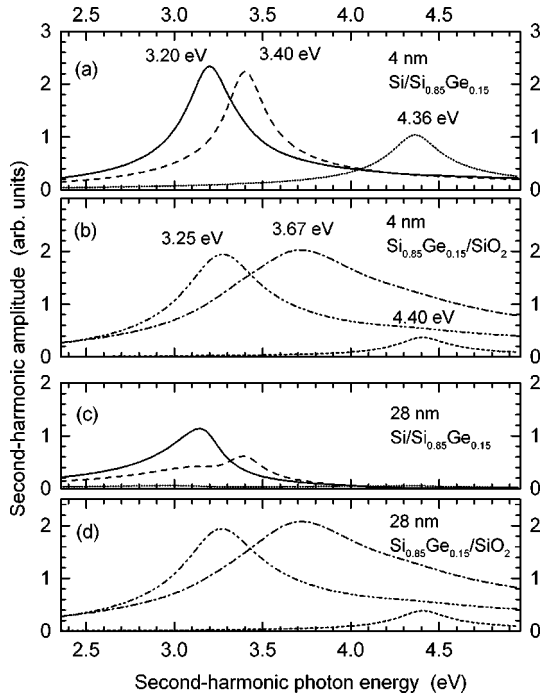

FIG. 10. Magnitude $|E_{1+}^{2\omega}|$ [see Eq. (7)] of the second-harmonic field amplitudes for the 4- and 28-nm samples, resolved as individual contributions from the three resonances of each interface. These field amplitudes were calculated from the fits assuming that only the interface tensor element $\chi_{s,zzz}^{(2)}$ contributes to the SHG. The resonance energies obtained from the fit are indicated. Note that the contributions from the alloy-substrate interface are virtually not affected by the thickness of the alloy layer.

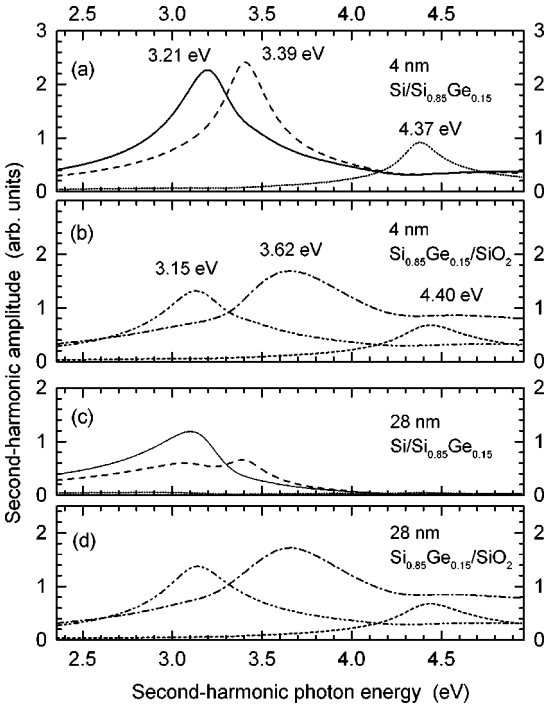

FIG. 11. Same as in Fig. 10, but for $\chi_{s,xxz}^{(2)}$.

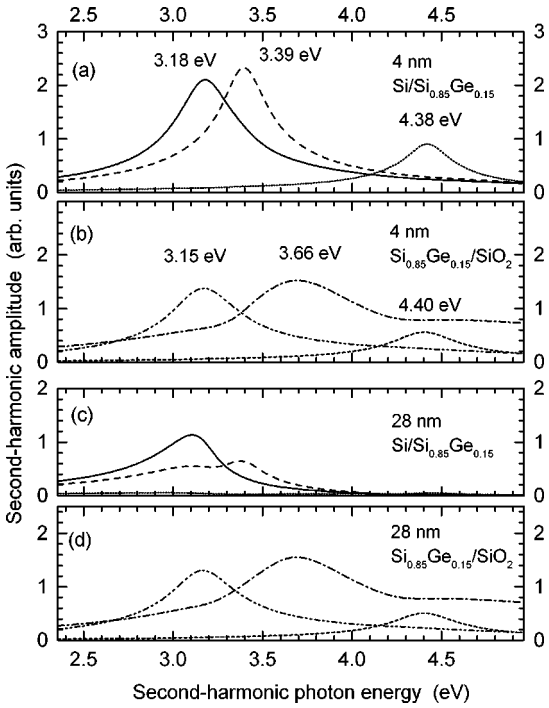

FIG. 12. Same as in Fig. 10 but for $\chi_{s,zxx}^{(2)}$. The SHG coefficient of $\chi_{s,xxz}^{(2)}$ was used for the resonance at 3.66 eV because this resonance was not observed in *s*-in/*p*-out spectra. A fit with the coefficient of $\chi_{s,zzz}^{(2)}$ for this resonance yielded energies of 3.19, 3.40, and 4.38 eV for the Si(100)-$Si_{0.85}Ge_{0.15}$ interface and 3.19, 3.64, and 4.40 eV for the $Si_{0.85}Ge_{0.15}$-SiO_2 interface.

from the different frequency dependencies of the coefficients $A_k(\omega,\theta)$ for the three interface tensor elements. Since we have no indication that one of the three tensor elements prevails in the spectra, we take the average of the energies and quote error margins that include the fitted resonance energies for all three elements.

The dominant contribution of the alloy-oxide interface is a strong, broad resonance around 3.65 ± 0.03 eV which was also observed at Si(100)-SiO_2 interfaces with energies between 3.6 and 3.8 eV.[8] This band was not detected in *s*-in/*p*-out spectra, and we therefore assigned it to the *zzz* and/or *xxz* components of $\chi_s^{(2)}$. It has no equivalent in the dielectric function of bulk crystalline silicon, and was not observed in previous studies using linear optical spectroscopies, presumably because of their much lower interface sensitivity. The energies of these transitions fall between the bulk E_1 and E_2 CP's, indicating considerable distortions of the tetrahedral bonding configuration at this interface that go beyond perpendicular lattice strains with tetragonal distortions. The latter would still lead to a spectral E_1/E_2 structure for the interband transitions.[8] We therefore assign this resonance to interband transitions involving those Si and Ge atoms which are closest to the $Si^{(+n)}$ atoms with oxidation levels $n>0$ forming the suboxide transition region, and which lack T_d symmetry as a consequence. As pointed out in Ref. 8, the large width of this resonance could be caused by a wide distribution of bond angles and lengths for these atoms.

The alloy-oxide interface also has bulk CP-type excitations around 3.19 ± 0.06 eV and 4.40 ± 0.06 eV.[30] The large error margin for the energy of the E_1-type resonance results from the large spread of the fitted resonance energies (3.15–

3.25 eV) for the three interface tensor elements. We have reason to believe that the strength of this resonance is largely overestimated in Figs. 10–12 for the following reason: as mentioned above, the 3.65-eV resonance is not well described by the excitonic line shape because of its long-range tails. As a consequence, the fits yielded an increased contribution of the alloy-oxide interface between 3.2 and 3.4 eV to compensate for this tail by destructive interference,[31] resulting in an apparent increase of amplitude, energy, and linewidth of the E_1 resonance. Since this effect is most pronounced for $\chi^{(2)}_{s,zzz}$ (Fig. 10) and less pronounced for $\chi^{(2)}_{s,xxz}$ and $\chi^{(2)}_{s,zxx}$ (Figs. 11 and 12), we consider an energy of 3.15 eV to be more representative of the E_1 excitations of this interface. This value is somewhat lower than the bulk E_1 energy of $Si_{0.85}Ge_{0.15}$ (3.19 eV), but consistent with a Ge enrichment at the interface due to SiO_2 formation.[32] Fits with a more realistic line shape for the resonance at 3.65 eV will yield more reliable parameters for the E_1 resonance of this interface.

A significant result is the strong blueshift of about 0.10 – 0.13 eV compared to the bulk value of $E_2(X)$, observed for the E_2-type resonances of both the alloy-oxide and substrate-alloy interfaces (*vide infra*). Similarly large values were also observed for Si(100)-SiO_2 interfaces,[8] consistent with the insensitivity of the bulk E_2 critical-point energy to variations of the Ge content.[3,4] This large blueshift cannot be related to the Ge content or to strain at the interface. We have speculated[8] that the E_2-derived bands at 4.4 eV of both Si and $Si_{1-x}Ge_x$ interfaces might contain significant contributions from $E_2(\Sigma)$-derived transitions which have an energy of about 4.5 eV in the bulk.[24] A definitive and conclusive explanation of this strong blueshift has yet not been presented, however. It should be noted that the E_2 excitations at the $Si_{0.85}Ge_{0.15}$-oxide interface are significantly weaker compared to the Si(100)-SiO_2 interface (Fig. 6). This is most obvious from the spectrum of the 28-nm sample in Fig. 8 which has no discernible contribution from the substrate-alloy interface in this energy range.

The Si(100)-$Si_{0.85}Ge_{0.15}$ interface has strong E_1-type resonances with energies of 3.40 ± 0.01 eV for the Si region and 3.20 ± 0.02 eV for the alloy region of the interface, as well as a weaker E_2 resonance at 4.37 ± 0.01 eV (Figs. 10–12). Note that the fits with the SHG coefficients of all three interface tensor elements yielded spectra with very similar energies, although linewidths and amplitudes depend somewhat on the tensor element. The E_1 energies, obtained from free fits, agree well with the respective bulk values of Si (3.40 eV) and strained $Si_{0.85}Ge_{0.15}$ (3.19 eV), and thus support the validity of our model for the frequency dependence of $\chi^{(2)}_s$ of this interface. Since the absorption in $Si_{0.85}Ge_{0.15}$ increases from 3.20 to 3.40 eV, the Si-derived E_1 transitions at the interface are more strongly attenuated than the transitions from the alloy side. This causes the apparent redshift of the E_1-type feature for increasing alloy thickness in Fig. 8.

A recent Raman study revealed that the bulk of epitaxial $Si_{1-x}Ge_x$ layers is homogeneously strained.[33] As a consequence, inhomogeneous lattice strain, which lifts the dipole rule for SHG in centrosymmetric media,[34] is confined to the near-interface region between the Si substrate and the homogeneously strained $Si_{0.85}Ge_{0.15}$ layer, which justifies our analysis of the spectra in terms of interface susceptibilities. In a recent work on short-period (Si_mGe_n) strained-layer superlattices, inhomogeneous strain was proposed to be responsible for an observed strong increase of the SHG intensity.[35] In that work the strain field was related to the formation of stacking faults when the thickness of the Ge layers in the superlattice exceeded the critical thickness h_c of about 6–7 ML. The contribution of defects to the SHG intensity should be comparatively small for our 4–28-nm strained layers with a Ge content of 15%, because the critical thickness is about 100 nm.[10] Furthermore, we observed the strongest SHG signal for the sample with the thinnest strained layer (4 nm), leaving an interpretation in terms of defect-enhanced SHG as unlikely. We therefore consider the specific structure of a well-ordered and defect-free Si(100)-$Si_{0.85}Ge_{0.15}$ interface as the primary source for the strong SHG signals around the E_1 energies in Fig. 8. We point out that inhomogeneous strain perpendicular to the interface is only one mechanism that breaks inversion symmetry at the Si(100)-$Si_{0.85}Ge_{0.15}$ interface and leads to dipole-allowed SHG. The gradient of the Ge concentration profile which extends over 2–3 atomic layers across the interface due to interdiffusion[36] represents a second mechanism that also lifts the structural inversion symmetry at this interface. At present we are not able to judge from our experimental data which of these two effects prevails.

The two resonance energies at 3.20 and 3.40 eV obtained from the fits can be considered as characteristic values for the E_1 interband transition energies, representing the respective sides of the Si(100)-$Si_{0.85}Ge_{0.15}$ interface region. We have also tried to model the SHG response of this interface with a single E_1 resonance (in addition to the E_2 resonance), representing the entire interface region. No satisfactory fit to the experimental spectra could be obtained with that model, however. In fact, our approach to describe the SHG response of the Si(100)-$Si_{0.85}Ge_{0.15}$ interface with three interband resonances turned out to be the model with a minimum of fit parameters for a reasonable reproduction of the measured spectra. Since our model yields realistic values for the E_1 and E_2 energies, we are confident that it represents a reasonable approximation for the SHG susceptibility of this interface. We have also checked the significance of additional transitions around 3.6 eV, in analogy to the alloy-oxide interface, and found only an unsignificant contribution consistent with the pseudomorphic structure of this interface. Therefore, the bulk-type resonances contain *all* interband transitions of this interface, thus giving rise to the strong SHG signal around the E_1 CP in Fig. 6. The phase difference between the E_1 contributions from the two adjacent interface regions is about 0.8π. This phase difference offers a simple explanation for the relative weakness of the E_2-derived band at 4.37 eV of the substrate-alloy interface: in contrast to the E_1 transitions, the E_2 transitions have the same energies in Si and $Si_{0.85}Ge_{0.15}$, and the partially destructive interference of the contributions by the two interface regions causes a decreased intensity of this interband resonance in the SHG spectrum. The relation between energies, phases, and strengths of the interband resonances and the profiles of Ge concentration and strain across the substrate-alloy interface should be an interesting issue for future SHG investigations of this system.

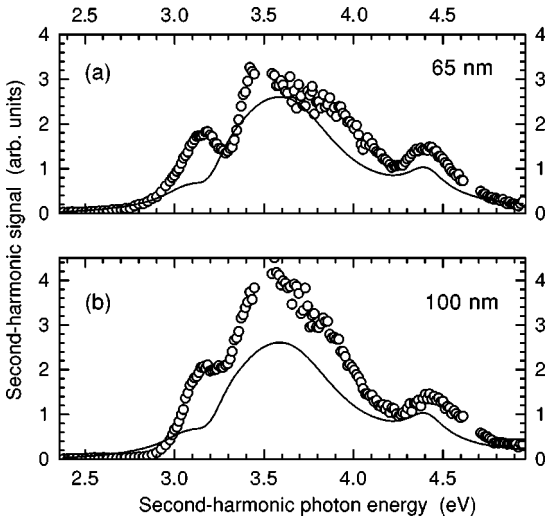

FIG. 13. SHG spectra of strained Si(100)-$Si_{0.85}Ge_{0.15}$-SiO_2 structures with (a) 65- and (b) 100-nm thicknesses of the alloy layer, respectively. Solid lines: SHG spectra calculated from the interband resonance parameters of the fit in Fig. 8.

D. Preliminary results for thick $Si_{0.85}Ge_{0.15}$ layers

In Fig. 13 we present SHG spectra of heterostructures with 65- and 100-nm alloy thickness, respectively. Calculated SHG spectra for 65 and 100 nm using the resonance parameters of the fit in Fig. 8 are also shown for comparison. Obviously the resonance parameters obtained from the fits to spectra with thin alloy layers do not describe the SHG spectra of heterostructures with thick $Si_{0.85}Ge_{0.15}$ layers in a quantitative way. We point out that the spectra of these samples are dominated by SHG at the alloy-oxide interface for energies larger than 3.2 eV, and that these spectra are very different from spectra of oxidized Si(100) surfaces (Fig. 6 and spectra in Ref. 8), the enhanced intensity around 3.5–3.6 eV being the most significant difference. These changes of the electronic structure at the alloy-oxide interface are presumably related to structural changes in the strained layers when the layer thickness approaches the critical thickness h_c for strain relaxation. For a more specific interpretation of these changes, the spectroscopic results have to be complemented by structural investigations.

V. CONCLUSION

We have presented a comprehensive investigation of SHG from Si(100)-$Si_{0.85}Ge_{0.15}$-SiO_2 heterostructures, and we have shown that various interband contributions of the two buried interfaces can be identified when spectra of samples with different thicknesses are analyzed. Analysis and interpretation of the data was facilitated by a strong variation of the SHG spectra with the thickness of the strained layers due to interference of the SHG waves generated at the two interfaces. Bulklike E_1- and E_2-type interband excitations dominate the contribution of the substrate-alloy interface to the spectra. Both the gradient of Ge concentration and inhomogeneous lattice strain across this interface represent symmetry-breaking elements that lift the dipole selection rule for SHG at this interface, causing the appearance of critical-point-like interband resonances in the SHG spectra. For the alloy-oxide interface we observed a type of interband excitations representing alloy atoms at the interface with strong bond distortions due to the presence of the adjacent suboxide. Our work demonstrates the advantages of the unrivaled interface sensitivity of SHG for the investigation of electronic excitations at buried interfaces, and we hope it will stimulate further studies of semiconductor interfaces using SHG spectroscopy.

[1] *Strained-Layer Superlattices: Materials Science and Technology*, edited by T. P. Pearsall, Semiconductors and Semimetals Vol. 33 (Academic, San Diego, 1991).
[2] E. Kasper, H. Kibbel, H.-J. Herzog, and A. Gruhle, Jpn. J. Appl. Phys. **33**, 2415 (1994).
[3] J. Humlíček, M. Garriga, M. I. Alonso, and M. Cardona, J. Appl. Phys. **65**, 2827 (1989).
[4] C. Pickering and R. T. Carline, J. Appl. Phys. **75**, 4642 (1994).
[5] T. F. Heinz, F. J. Himpsel, E. Palange, and E. Burstein, Phys. Rev. Lett. **63**, 644 (1989).
[6] M. S. Yeganeh, J. Qi, A. G. Yodh, and M. C. Tamargo, Phys. Rev. Lett. **68**, 3761 (1992).
[7] W. Daum, H.-J. Krause, U. Reichel, and H. Ibach, Phys. Rev. Lett. **71**, 1234 (1993).
[8] G. Erley and W. Daum, Phys. Rev. B **58**, R1734 (1998).
[9] R. Butz and S. Kampers, Appl. Phys. Lett. **61**, 1307 (1992).
[10] Y. Kohama, Y. Fukuda, and M. Seki, Appl. Phys. Lett. **52**, 380 (1988).
[11] G. Erley, Ph. D. thesis, RWTH Aachen, 1997.
[12] H.-J. Krause and W. Daum, Appl. Phys. B: Photophys. Laser Chem. **56**, 8 (1993).
[13] J. I. Dadap, P. T. Wilson, M. H. Anderson, M. C. Downer, and M. ter Beek, Opt. Lett. **22**, 901 (1997).
[14] S. K. Kurtz and T. T. Perry, J. Appl. Phys. **39**, 3798 (1968).
[15] The measured SHG spectra from the urea reference sample were normalized to the SHG signal simultaneously recorded from a crystalline quartz plate. The frequency dependence of the nonlinear susceptibility of quartz was assumed to obey Miller's rule.
[16] J. E. Sipe, D. J. Moss, and H. M. van Driel, Phys. Rev. B **35**, 1129 (1987).
[17] J. E. Sipe, J. Opt. Soc. Am. B **4**, 481 (1987).
[18] P. Guyot-Sionnest, W. Chen, and Y. R. Shen, Phys. Rev. B **33**, 8254 (1986).
[19] C. H. Lee, R. K. Chang, and N. Bloembergen, Phys. Rev. Lett. **18**, 167 (1967).
[20] O. A. Aktsipetrov, I. M. Baranova, K. N. Evtyukhov, T. V. Murzina, and I. V. Chernyĭ, Sov. J. Quantum Electron. **22**, 807 (1992).
[21] J. I. Dadap, X. F. Hu, M. H. Anderson, M. C. Downer, J. K. Lowell, and O. A. Aktsipetrov, Phys. Rev. B **53**, R7607 (1996).
[22] I. H. Malitson, J. Opt. Soc. Am. **55**, 1205 (1965).
[23] Y. R. Shen, *The Principles of Nonlinear Optics* (Wiley, New York, 1984), p. 18.
[24] P. Lautenschlager, M. Garriga, L. Viña, and M. Cardona, Phys. Rev. B **36**, 4821 (1987).
[25] W. H. Press, B. P. Flannery, S. A. Teukolsky, and W. T. Vetter-

ling, *Numerical Recipes in Pascal* (Cambridge University Press, Cambridge, 1992).

[26] R. People and J. C. Bean, Appl. Phys. Lett. **48**, 538 (1986).

[27] S. Bergfeld and W. Daum (unpublished).

[28] D. J. Bottomley, G. Lüpke, M. L. Ledgerwood, X. Q. Zhou, and H. M. van Driel, Appl. Phys. Lett. **63**, 2324 (1993).

[29] The E_1 energy of relaxed $Si_{0.85}Ge_{0.15}$ is 3.18 eV (Ref. 3). From the spin-orbit-splitting, the deformation potentials, and the elastic constants, one calculates a stress-induced blueshift of about 10 meV for the E_1 energy of strained $Si_{0.85}Ge_{0.15}$ layers (Ref. 11).

[30] We note that the energy of this interband resonance was actually not obtained from the fits but was kept fixed at a value of 4.40 eV. Because of the weak contribution of this resonance to the spectra, a free fit shifted its energy to an unrealistically large value without improving the quality of the fit. A reduction of this energy towards the bulk E_2 energy of 4.27 eV clearly worsened the fits. In our investigations of various Si(100)-SiO_2 interfaces (Refs. 8 and 11), we found the energy of this resonance to lie between 4.34 and 4.45 eV. Correspondingly, we give an error margin of ± 0.06 eV for the energy of this resonance.

[31] The phase difference between these two resonances is about 0.9π.

[32] Y. Yin, F. H. Pollak, P. Auvray, D. Dutartre, H. Pantel, and J. A. Chroboczek, Thin Solid Films **222**, 85 (1992).

[33] F. Lu, C. H. Perry, F. Namavar, N. L. Rowell, and R. A. Soref, Appl. Phys. Lett. **63**, 1243 (1993).

[34] S. V. Govorkov, V. I. Emel'yanov, N. I. Koroteev, G. I. Petrov, I. L. Shumay, and V. V. Yakovlev, J. Opt. Soc. Am. B **6**, 1117 (1989).

[35] C. Zhang, X. Xiao, N. Wang, K. K. Fung, M. M. T. Loy, Z. Chen, and J. Zhou, Appl. Phys. Lett. **72**, 2072 (1998).

[36] R. Schorer, G. Abstreiter, S. de Gironcoli, E. Molinari, H. Kibbel, and H. Presting, Phys. Rev. B **49**, 5406 (1994).